New insights into photodynamic therapy treatment through the use of 3D Monte Carlo radiation transfer modelling.

C. Louise Campbell[a], Kenneth Wood [a], C. Tom A. Brown[a] and Harry Moseley[b]

[a]SUPA, School of Physics and Astronomy, University of St Andrews, UK;
[b]Photobiology Unit, Ninewells Hospital and Medical School, University of Dundee, UK

ABSTRACT

Photodynamic therapy (PDT) has been theoretically investigated using a Monte Carlo radiation transfer (MCRT) model. By including complex three dimensional (3D) tumour models a more appropriate representation of the treatment was achieved. The 3D clustered tumour model was compared to a smooth model, resulting in a significantly deeper penetration associated with the clustered model. The results from the work presented here indicates that light might penetrate deeper than suggested by 2D or simple layered models.

Keywords: Monte Carlo radiation transfer, Photodynamic therapy, skin optics, daylight PDT, fractal model, non-homogeneous tumour model

1. INTRODUCTION

Photodynamic therapy (PDT) relies on the interaction between light, a photosensitive chemical and molecular oxygen to kill targeted cells. This non-invasive treatment method provides an efficient way of topically treating skin lesions such as non-melanoma skin cancer (NMSC) and precancerous lesions including Basal Cell Carcinoma (BCC), Aktinic Keratosis (AK) and Bowen's disease (BD). Through selective accumulation of the photosensitiser in tumour cells, the treatment achieves an interaction where healthy tissue surrounding the lesion is largely unaffected. For topical PDT, a prodrug in the form of a cream is topically applied to the lesion prior to the irradiation of light. The cream contains either 5-aminolaevulinic acid (ALA) or methyl aminolevulinate (MAL), which is converted within the tumour cells into the photosensitive molecules Protoporphyrin IX (PpIX).[1,2]

The PpIX absorbes light over a wide range of wavelengths. It is common however to target the small absorption peak at around 630 nm to achieve deep penetration of the excitation radiation. Recent studies have shown that alternative light sources such as daylight, can achieve sufficient treatment depths for eradicating superficial skin lesions such as AKs.[3,4] By utilising the whole absorption spectrum of the photosensitiser a lower irradiance is required to achieve the same absorption. Even though this results in a slightly more shallow treatment due to the dominating absorbing features of PpIX in the blue wavelength range (figure 1 c) many efficient results have been reported.[5–9] Daylight has been shown to be associated with a lower experienced pain[10] and the preferred choice of treatment by the majority of patients.[3] In the work presented here we compare daylight PDT to conventional PDT where the artificial light source Aktilite is adopted (Akitlite, Photocure ASA, Norway[11]).

To further investigate the light interaction with skin tissue during the treatment, theoretical models are commonly adopted. Monte Carlo radiation transfer (MCRT) modelling is the gold standard when simulating light transport through skin tissue. MCRT provides a flexible method which generates accurate information of the light distribution, scattering and absorption events within the skin tissue during illumination. The majority of MCRT models simulating PDT assume uniform distributions of skin tissue.[12] Some models introduce layers of different tissue types and/or tumours represented by geometric shapes. However, within the confined areas, the distribution of the tissue type is uniform. Here a 3D MCRT model is introduced where the tumour is represented by a hierarchical structure, regrouping the density of the tumour into clusters. This allows for the 3D features of the model to be explored and provides important information about the relevance of including a 3D system.

Further author information: (Send correspondence to C L Campbell)
C L Campbell: E-mail: clc57@st-andrews.ac.uk, Telephone: +44(0)753 1417790

Photonic Therapeutics and Diagnostics XII, edited by Bernard Choi, et al., Proc. of SPIE
Vol. 9689, 96890Q · © 2016 SPIE · CCC code: 1605-7422/16/$18 · doi: 10.1117/12.2212240

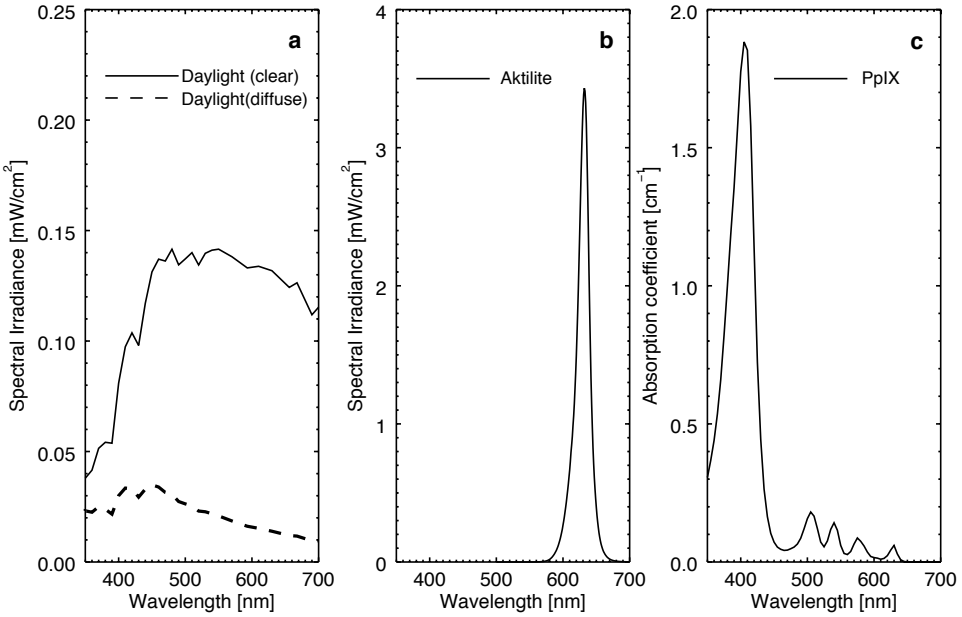

Figure 1: Figure showing the spectra included in the theoretical model. a) Spectral irradiance of the two daylight components. Direct daylight (solid) has a defined directionality while the diffuse daylight (dashed) is assumed to not have a defined directionality.[13] b) Spectral irradiance of the conventional light source (Aktilite) adopted in the model. c) Absorption spectrum of the photosensitiser PpIX corresponding to the smooth initial number density of PpIX molecules equal to $7.84 \times 10^{13}\,\mathrm{cm}^{-3}$. However the absorption properties vary depending on the concentration of the PpIX within the tumour tissue.[14,15]

2. METHODS

The radiative transfer equation (RTE) describes the propagation of photons through any medium.[16] Due to the difficulty in solving the equation, several approximations have been developed. MCRT is a numerical technique which simulates the light distribution through a highly scattering media by utilising the probabilistic nature of the photon interactions. This technique accurately describes the propagation of light through skin tissue and has several times been used to simulated light therapies such as PDT.[17,18] The code that is presented here has been developed from a publicly available code has been thoroughly validated.[4,19]

2.1 Monte Carlo radiation transfer

The MCRT code tracks energy packets (hereafter referred to as photons) as they propagate through their propagation through a 3D Cartesian grid containing voxels. By allocating appropriate optical properties to each voxel, the scattering and absorption events are accurately represented. These events are recorded by conributing to counters containing information about the energy deposition and light distribution. The photons are tracked through the grid until they are either absorbed or scattered out of the simulated region. By repeating the process for multiple photons the results approach the true representation. The optical properties within each voxel can differ from adjacent voxels, which allows for complicated 3D structures to be included. This was utilised in our work to include complex 3D tumour structures that were subsequently compared to models where the tumour was assumed to have a uniform density.

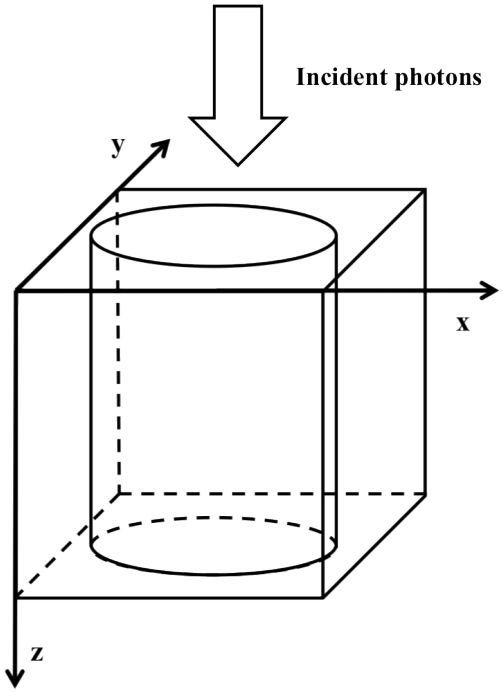

Figure 2: Figure demonstrating the Cartesian grid that was simulated to represent the skin tissue. Within the cube a cylindrical tumour with a diameter of 6 mm was included. The length of each side of the cube was set to be 10 mm. The density of the tumour model was assumed to be uniform throughout the tumour for the smooth model. For the fractal model the density was rearranged within the cylinder with the average density throughout the cylinder was the same.

2.2 Code set up

The grid system was assumed to be uniformly illuminated from above (figure 2). The grid contained $101\times101\times101$ voxels with the dimensions $10\,\text{mm}\times10\,\text{mm}\times10\,\text{mm}$. The optical properties that were adopted are displayed in figure 3. These determine the probability of a scattering or absorption event occurring at an interaction event. The Heyney-Greenstein phase function[20] was adopted to describe the scattering angular distribution where the anisotropy factor was assumed to follow the wavelength dependency, $g = 0.62+\lambda\times0.29\times10^{-3}$ (with λ in nm).[21] The refractive index was assumed to be uniform for all tissue types (n=1.38) and the refraction and reflection at the upper boundary was considered using Snell's law and Fresnel reflectance.

Repeated boundaries were adopted to represent a semi-infinate tissue slab. 3D wavelength dependent photobleaching depending on both fluence rate and initial concentration of PpIX was included to consider the destruction of PpIX during the illumination.[4] It was assumed that there was an unlimited oxygen supply and the PpIX was assumed to only be present within the tumour areas.

The fluence rate was generated for three wavelengths, 405, 540 and 630 nm to compare different parts of the spectra. In addition the photodynamic dose (PDD) was generated for both conventional and daylight PDT where the PDD is defined as the number of absorbed photons by the photosensitiser per unit volume.[25] The PDD is assumed to be proportional to the number of produced singlet oxygen molecules and a toxic threshold can therefore be considered. This allows for an estimation of the efficient treatment depth and means of comparing different light sources and treatment conditions.[26] For illustrative purposes a threshold of 8.6×10^{17} photons cm^{-3} was adopted to enable the comparison between the different treatment modalities considered.[17] The effect of including a fractal clustered model (section 2.4) and a smooth model was compared for both daylight as well as conventional PDT.

The fluorescence generated by 405 nm excitation was simulated by assuming that each absorption by the

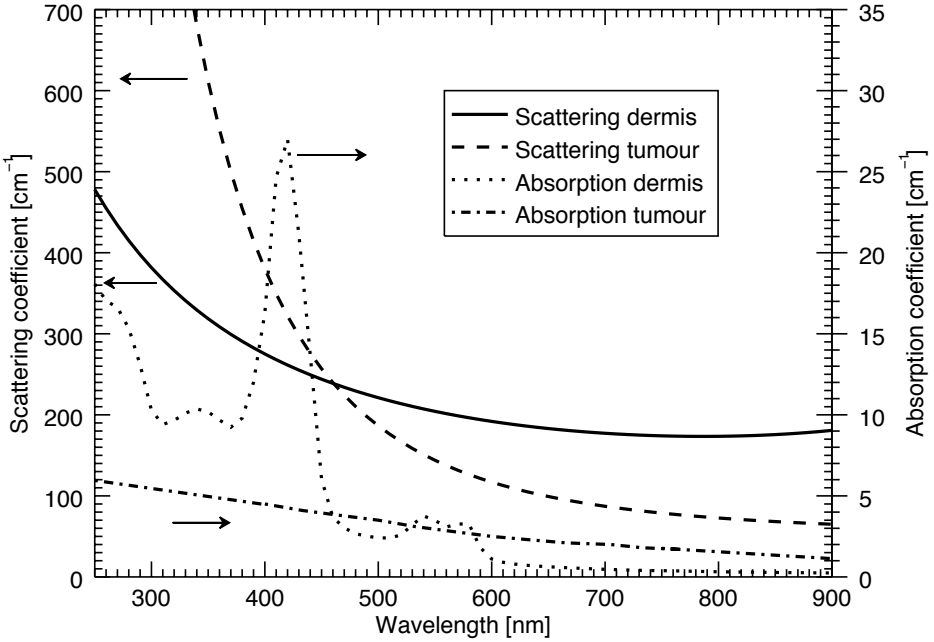

Figure 3: Figure showing the optical properties implemented within the theoretical model. Both the absorption and scattering properties of the healthy and diseased tissue are included within the figure. The optical properties were generated from algorithms presented by Yudovsky et al[22,23] as well as from data extracted from Salomatina et al[24] using the approach developed by Jacques et al.[17]

PpIX resulted in a fluorescence photon. The fluorescence photon was assumed to be isotropically reemitted from the absorption location at a wavelength sampled from the spectra shown in figure 4. All fluorescence photons escaping from the surface of the grid was recorded, generating a simulation of the expected wide field fluorescence image.

2.3 Light sources

The spectral distribution of the different light sources investigated are displayed in figure 1. The conventional treatment methods assumed a vertical illumination with the irradiance of 82 mW cm^{-2}. For daylight PDT both the direct and diffuse component of the light source had to be considered. To simulate a clear day it was assumed that 80 % of the light was direct while 20 % was assumed to be diffuse light. The direct light was assumed to have a defined directionality and illuminate the surface of the skin at an angle of 30 degrees (from the normal) and the diffuse component was assumed to not have any defined directionality. This was considered by randomly allocating a direction of illumination for each photon, resulting in a uniformly diffuse illumination of the surface of the skin. It is possible to simulate different weather conditions by changing the ration between the direct and tissue component however here we only considered the clear case. The irradiance of the clear daylight case was determined to be 41 mW cm^{-2}. These values for the daylight are equivalent to those observed at noon in summer at a latitude of 56 degrees North.[4]

The wavelength of the simulated photon was randomly determined from the light spectra such that the probability distribution function of the illuminating spectra is reproduced. Hence the allocated wavelength depends on the spectral distribution of the light source (figure 1).

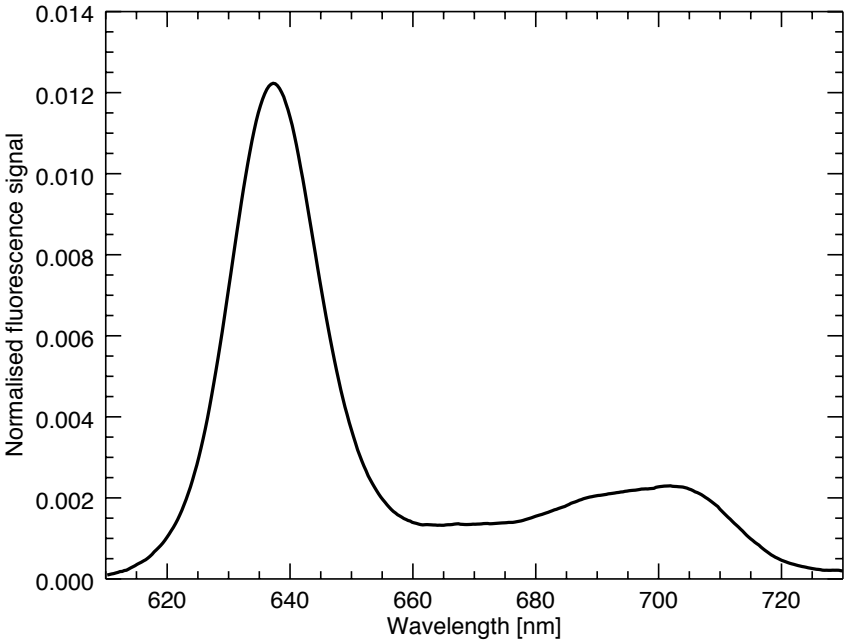

Figure 4: Figure showing the fluorescent spectra generating by the PpIX.

2.4 Tumour models

The original model consisted of a symmetric grid system containing a cylindrical tumour in the centre and has been adopted in our previous work (figure 2).[4] Within the cylindrical tumour, the density was assumed to have a uniform distribution. This smooth model was compared to a fractal model where the density of the tumour tissue was rearranged such that the average density throughout the tumour region was the same as the smooth model. The motivation for using a clustered model is to demonstrate what is believed to be a more complex and potentially a more realistic model of a tumour structure. Through histopathological images[27] of skin lesions, the clustered model appears to be an appropriate initial step into modelling different tumour structures.

The 3D clustered structure was determined using the algorithm presented by Elmegreen (1997).[28] Four levels of the algorithm is adopted. At the first level, 128 points are determined within the 3D coordinate system. At the next level 128 points were cast around each individual point from the previous level. This was then repeated for a total of four levels generating a fractal model. The distance of the subsequent level from the previous level reduces with the increased hierarchical level. For a more details description of the complex clustered model, see Wood et al (2005).[29] The algorithm restructures the density and for the model presented here 70 % of the tumour was assumed to be within the clustered features while the remaining 30 % was defined as the smooth component which comprises the remaining area around the different clusters. Figure 5 shows both the surface of the clustered model (a) as well as a slice of the tumour in the vertical plane (b).

The initial distribution of PpIX was assumed to be distributed identical to that of the tumour tissue. Hence for the smooth model the initial distribution of PpIX was assumed to be uniform within the cylindrical tumour while for the fractal case the PpIX was assumed to have an initial distribution identical to the fractal model. For the purpose of this work the PpIX was assumed to not be present within the healthy tissue surrounding the tumour. It was assumed that the tissue surrounding the tumour was of a single tissue type (dermis) and of

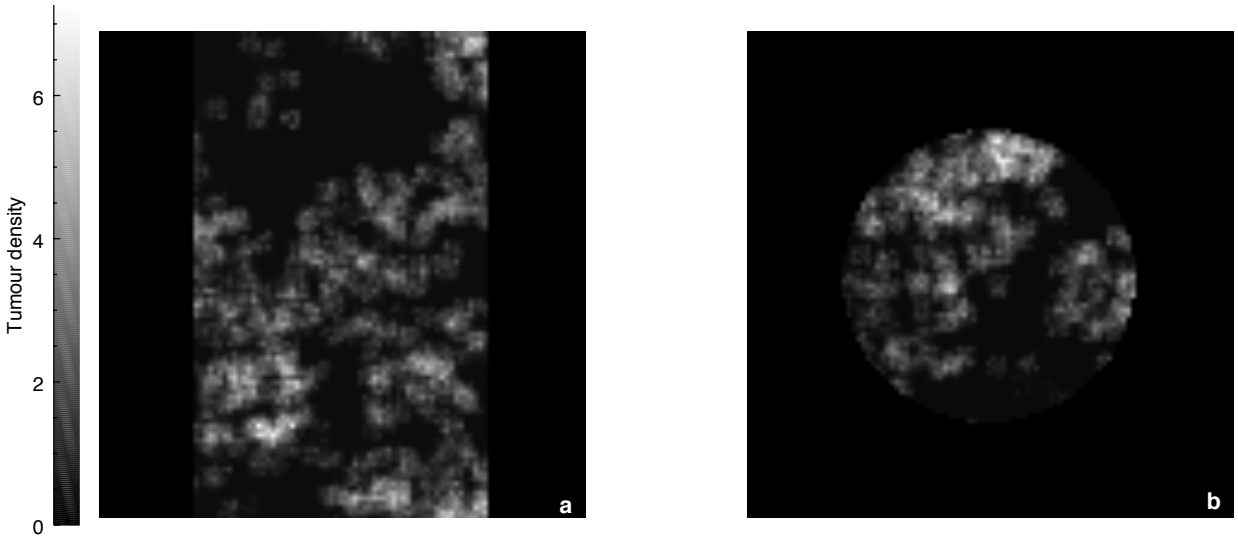

Figure 5: b) Figure showing a slice of the tumour, where the density was regrouped within the cylindrical tumour. a) Figure showing the top of the grid, displaying the surface of the developed tumour structure. 70 % of the density was regrouped into the clustered features while 30 % of the total tumour content was smoothly distributed throughout the cylinder. It was assumed that the photosensitiser PpIX is only contained within the tumour tissue.

smooth uniform density.

3. RESULTS

The penetration of light is highly wavelength dependent and this is demonstrated in figure 6 where the fluence rate for three different wavelengths is displayed. The figure demonstrates the average over the whole cylindrical area. Both the fractal and the smooth models are compared for the three wavelengths and it is clear that there is a large difference between the two different models. The fractal model results in deeper penetration due to the clusters generating gaps of lower density. The fluence rate also demonstrates how the light penetrated deeper for the longer wavelength (630 nm) which is a wavelength typical used for conventional PDT.

Figure 7 shows the PDD for daylight (during clear conditions) as well as conventional PDT. The figure demonstrates the accumulated PDD after a delivered light dose of 75 $\mathrm{J\,cm^{-2}}$ which results in different treatment time for the different light conditions. This is a typical light dose delivered for conventional PDT treatments and therefore the light dose compared. Both the fractal model and the smooth model are compared demonstrating the significantly deeper penetration arising from the fractal model. The horizontal line in figure 7 represents the toxic threshold. The results indicate an additional 0.5 mm gained in treatment depth, by considering a complex 3D tumour structure.

The fluorescence image generated by the simulation is shown in figure 8. This differs from the density image in figure 5 since it considers fluorescence light from below the surface of the tumour.

4. DISCUSSION

The introduction of a clustered 3D tumour model gives a more reasonable representation of the physical situation. This is the first time 3D features of light distribution of skin tissue have been explored. Previous symmetric shapes does not introduce the properties demonstrated here. By regrouping the tumour and PpIX density the light is allowed to penetrate deeper due to the added areas of reduced density. There is also an overall higher accumulated absorption at the surface due to the nature of the fractal model.

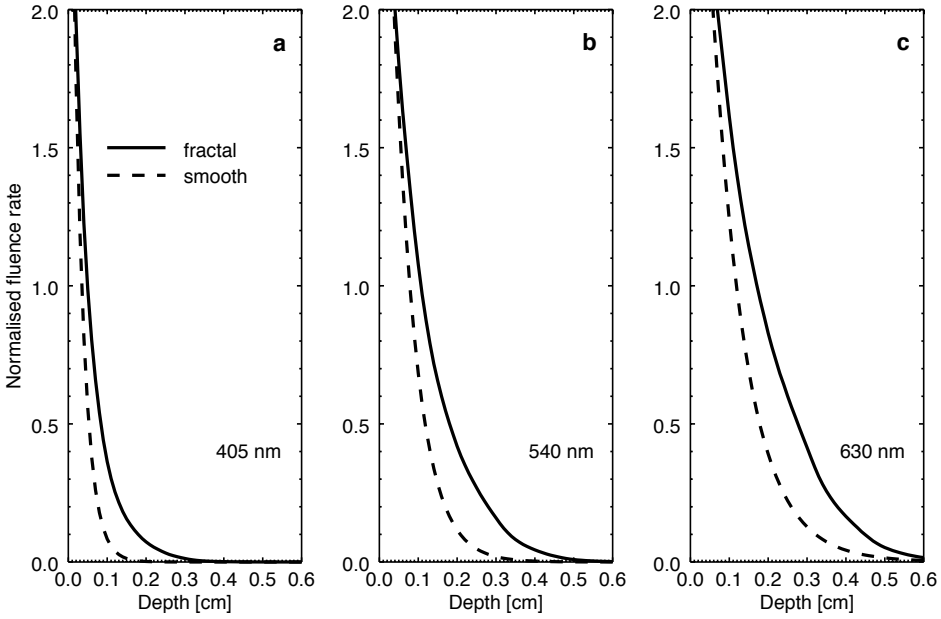

Figure 6: Figure showing the fluence rate for three different wavelengths a) 405 nm, b) 540 nm and c) 630 nm. For all three wavelengths the clustered model (solid) is compared to the equivalent smooth model (dashed).

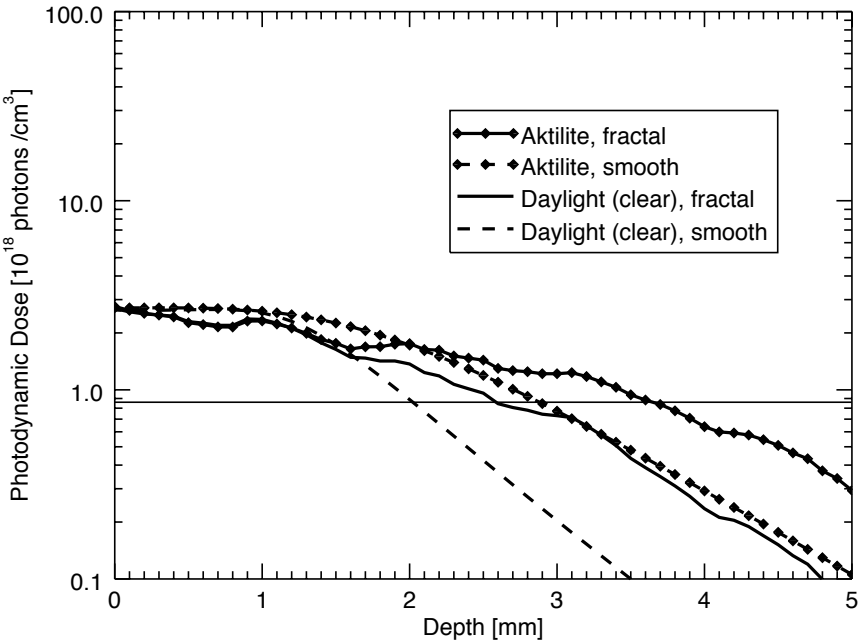

Figure 7: Figure showing the PDD for daylight PDT (during clear conditions) as well as conventional PDT (Aktilite). The clustered model is compared to the equivalent smooth model. The figure demonstrates the increase in effective treatment depth where the tumour density is redistributed according to figure 5.

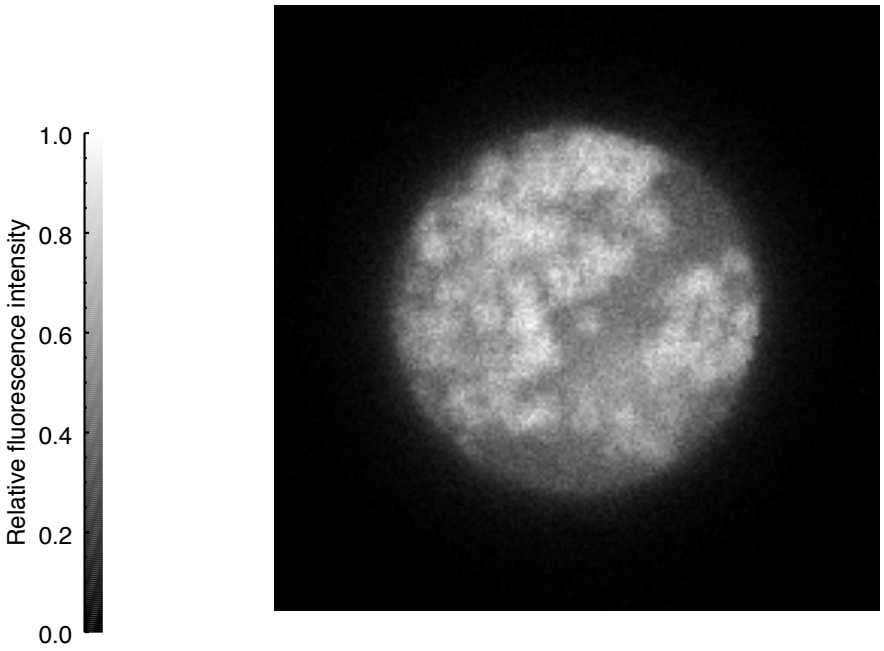

Figure 8: Image of the fluorescence light escaping from the tumour when illuminated with 405 nm light. The intensity of the fluorescence light is normalised such that only the relative intensity is displayed in the image.

The tumour model described here is produced through a mathematical algorithm and will therefore not be a true representation of tumour tissue. Even so, the added complexity shows the requirement of a 3D model when studying light distribution through skin tissue where the distribution in all directions play an important role. It has previously been suggested that two dimensional (2D) models are sufficient for representing the light propagation, however the work presented here shows the importance of including a more complicated model. Further developments of the model will include additional 3D tumour structures as well as a more detailed representation of the healthy tissue surrounding the tumour.

ACKNOWLEDGMENTS

We acknowledge the support of the UK Engineering and Physics Sciences Research Council (EPSRC) for funding through a studentship for C L Campbell (EP/K503162/1), the Alfred Stewart Trust as well as the BMLA Education Award.

REFERENCES

[1] Darlenski, R. and Fluhr, J., "Photodynamic therapy in dermatology: past, present, and future," *Journal of Biomedical Optics* **18**(6), 061208–061208 (2012).

[2] Castano, A., Demidova, T., and Hamblin, M., "Mechanisms in photodynamic therapy: part one - photosensitizers, photochemistry and cellular localization," *Photodiagnosis and Photodynamic Therapy* **1**(4), 279 – 293 (2004).

[3] Morton, C., Wulf, H., Szeimies, R., Gilaberte, Y., Basset-Seguin, N., Sotiriou, E., Piaserico, S., Hunger, R., Baharlou, S., Sidoroff, A., et al., "Practical approach to the use of daylight photodynamic therapy

with topical methyl aminolevulinate for actinic keratosis: a european consensus," *Journal of the European Academy of Dermatology and Venereology* (2015).

[4] Campbell, C., Wood, K., Valentine, R., Brown, C., and Moseley, H., "Monte carlo modelling of daylight activated photodynamic therapy," *Physics in medicine and biology* **60**(10), 4059 (2015).

[5] Wiegell, S., Heydenreich, J., Fabricius, S., and Wulf, H., "Continuous ultra-low-intensity artificial daylight is not as effective as red led light in photodynamic therapy of multiple actinic keratoses," *Photodermatology, Photoimmunology Photomedicine* **27**(6), 280–285 (2011).

[6] Wiegell, S., Fabricius, S., Stender, I., Berne, B., Kroon, S., Andersen, B., Mork, C., Sandberg, C., Jemec, G., Mogensen, M., Brocks, K., Philipsen, P., Heydenreich, J., Hdersdal, M., and Wulf, H., "A randomized, multicentre study of directed daylight exposure times of 1 1/2 vs. 2 1/2 h in daylight-mediated photodynamic therapy with methyl aminolaevulinate in patients with multiple thin actinic keratoses of the face and scalp," *British Journal of Dermatology* **164**(5), 1083–1090 (2011).

[7] Wiegell, S., Hadersdal, M., Eriksen, P., and Wulf, H., "Photodynamic therapy of actinic keratoses with 8% and 16% methyl aminolaevulinate and home-based daylight exposure: a double-blinded randomized clinical trial," *British Journal of Dermatology* **160**(6), 1308–1314 (2009).

[8] Fargnoli, M., Piccioni, A., Neri, L., Tambone, S., Pellegrini, C., and Peris, K., "Conventional vs. daylight methyl aminolevulinate photodynamic therapy for actinic keratosis of the face and scalp: an intra-patient, prospective, comparisonstudy in italy," *Journal of the European Academy of Dermatology and Venereology* **29**(10), 1926–1932 (2015).

[9] Lacour, J.-P., Ulrich, C., Gilaberte, Y., Von Felbert, V., Basset-Seguin, N., Dreno, B., Girard, C., Redondo, P., Serra-Guillen, C., Synnerstad, I., Tarstedt, M., Tsianakas, A., Venema, A., Kelleners-Smeets, N., Adamski, H., Perez-Garcia, B., Gerritsen, M., Leclerc, S., Kerrouche, N., and Szeimies, R.-M., "Daylight photodynamic therapy with methyl aminolevulinate cream is effective and nearly painless in treating actinic keratoses: a randomised, investigator-blinded, controlled, phase iii study throughout europe," *Journal of the European Academy of Dermatology and Venereology* , n/a–n/a (2015).

[10] Wiegell, S., Skiveren, J., Philipsen, P., and Wulf, H. C., "Pain during photodynamic therapy is associated with protoporphyrin ix fluorescence and fluence rate," *British Journal of Dermatology* **158**(4), 727–733 (2008).

[11] Moseley, H., "Light distribution and calibration of commercial pdt led arrays," *Photochem. Photobiol. Sci.* **4**, 911–914 (2005).

[12] Zhu, C. and Liu, Q., "Review of monte carlo modeling of light transport in tissues," *Journal of Biomedical Optics* **18**(5), 050902–050902 (2013).

[13] Bird, R. and Riordan, C., "Simple Solar Spectral Model for Direct and Diffuse Irradiance on Horizontal and Tilted Planes at the Earth's Surface for Cloudless Atmospheres," *Journal of Applied Meteorology* **25**, 87–97 (1986).

[14] Valentine, R., Brown, C. T. A., Moseley, H., Ibbotson, S., and Wood, K., "Monte carlo modeling of in vivo protoporphyrin ix fluorescence and singlet oxygen production during photodynamic therapy for patients presenting with superficial basal cell carcinomas," *Journal of Biomedical Optics* **16**(4), 048002–048002–11 (2011).

[15] Valentine, R. M., Ibbotson, S., Wood, K., Brown, C., and Moseley, H., "Modelling fluorescence in clinical photodynamic therapy," *Photochem. Photobiol. Sci.* **12**, 203–213 (2013).

[16] Yoon, G., Welch, A., Motamedi, M., and Gemert, M., "Development and application of three-dimensional light distribution model for laser irradiated tissue," *Quantum Electronics, IEEE Journal of* **23**, 1721–1733 (Oct 1987).

[17] Jacques, S., Alter, C., and Prahl, S., "Angular dependence of HeNe laser light scattering by human dermis," *Lasers Life Sci.* **1**, 309–333 (1987).

[18] Premru, J., Milani, M., and Majaron, B., "Monte carlo simulation of radiation transfer in human skin with geometrically correct treatment of boundaries between different tissues," *Proc. SPIE* **8579**, 85790Z–85790Z–13 (2013).

[19] Campbell, C. L., Christison, C., Brown, C. T. A., Wood, K., Valentine, R. M., and Moseley, H., "3d monte carlo radiation transfer modelling of photodynamic therapy," in [*SPIE Biophotonics South America*], 95311H–95311H, International Society for Optics and Photonics (2015).

[20] Henyey, L. and Greenstein, J., "Diffuse radiation in the Galaxy," **93**, 70–83 (Jan. 1941).
[21] Van Gemert, M., Jacques, S., Sterenborg, H., and Star, W. M., "Skin optics," *Biomedical Engineering, IEEE Transactions on* **36**(12), 1146–1154 (1989).
[22] Yudovsky, D. and Pilon, L., "Rapid and accurate estimation of blood saturation, melanin content, and epidermis thickness from spectral diffuse reflectance," *Appl. Opt.* **49**, 1707–1719 (Apr 2010).
[23] Yudovsky, D. and Pilon, L., "Retrieving skin properties from in vivo spectral reflectance measurements," *Journal of Biophotonics* **4**(5), 305–314 (2011).
[24] Salomatina, E., Jiang, B., Novak, J., and Yaroslavsky, A. N., "Optical properties of normal and cancerous human skin in the visible and near-infrared spectral range," *Journal of Biomedical Optics* **11**(6), 064026–064026–9 (2006).
[25] Jacques, S., Joseph, R., and Gofstein, G., "How photobleaching affects dosimetry and fluorescence monitoring of pdt in turbid media," *Proc. SPIE* **1881**, 168–179 (1993).
[26] Farrell, T., Hawkes, R., Patterson, M., and Wilson, B., "Modeling of photosensitizer fluorescence emission and photobleaching for photodynamic therapy dosimetry," *Appl. Opt.* **37**, 7168–7183 (Nov 1998).
[27] Scheibe, P., Braumann, U.-D., Kuska, J.-P., Lffler, M., Simon, J. C., Paasch, U., and Wetzig, T., "Image-processing chain for a three-dimensional reconstruction of basal cell carcinomas*," *Experimental Dermatology* **19**(7), 689–691 (2010).
[28] Elmegreen, B. G., "Intercloud Structure in a Turbulent Fractal Interstellar Medium," **477**, 196–203 (Mar. 1997).
[29] Wood, K., Haffner, L., Reynolds, R., Mathis, J. S., and Madsen, G., "Estimating the porosity of the interstellar medium from three-dimensional photoionization modeling of h ii regions," *The Astrophysical Journal* **633**(1), 295 (2005).